Thermal wave interferometry: a potential application of the photoacoustic effect

C. A. Bennett, Jr., and R. R. Patty

The Rosencwaig-Gersho equation for the photoacoustic signal is recast in a manner that emphasizes the crucial role thermal wave interference plays in the production of the photoacoustic signal. This formalism is then used to suggest a technique for extracting thermal information from the structure in the photoacoustic signal resulting from thermal wave interference. Experimental measurements illustrating this technique are presented.

I. Introduction

Early in the course of a photoacoustic study of elemental carbon this laboratory noticed a dependence of the photoacoustic signal on chopping frequency that introduced some unexpected structure in our data; this structure has subsequently been explained[1,2] in terms of the interference of thermal waves generated within samples that are not thermally thick. (The term thermal wave interference is used to mean the superposition of simple harmonic solutions of the thermal diffusion equation. Although wavelike in nature[3] there are important differences[4] between thermal waves arising from a differential equation that is of the first order in time and waves that are solutions to a wave equation that is of the second order in time.) It has always been clear that the information provided by this structure would be useful in analyzing thicknesses or thermal properties of thin film layers, and in this paper we describe a technique by which this information might be extracted in a straightforward manner. The technique consists of varying the wavelength of the thermal waves generated within a thin film sample by varying the modulation frequency of the incoming light and normalizing the photoacoustic signal by using the signal of a thermally thick sample of the same material to remove the effects of cell resonances, microphone response, etc. In this way the structure resulting from thermal wave interference may be studied unambiguously, and the analysis of these data will yield the properties of the thermal waves and of the medium in which they travel.

As will become clear presently thermal wave interference effects manifest themselves most predominantly in samples that are very thin thermally. For this range of sample thicknesses and modulation frequencies we expect thermoelastic stress waves to contribute negligibly to the photoacoustic signal, and we therefore use the theory of Rosencwaig and Gersho[5] as a theoretical foundation. Although thermal wave interference is implicitly contained in the Rosencwaig-Gersho theory, their result is recast in a manner that explicitly illustrates the role of this interference in the production of the photoacoustic signal by using an approach that incorporates the boundary conditions into thermal wave reflection and transmission coefficients. This equation will then be used to characterize the technique outlined above with a minimum number of internal parameters so that simplifying assumptions, if applicable, may be applied with greater accuracy. The special case of an opaque sample and reference is considered, and theoretical results are displayed in plots of photoacoustic signal and phase vs thermal thickness. We conclude by using samples of particulate carbon to demonstrate the technique experimentally, to illustrate the role of the backing material in this process, and finally to verify that the structure observed is indeed due to thermal wave interference.

II. Theory

The photoacoustic signal arises from the energy absorbed from an amplitude modulated beam of light that impinges on the sample. This absorbed energy initiates rapidly damped traveling thermal waves within the sample, and the resulting thermal wave which is

The authors are with North Carolina State University, Physics Department, Raleigh, North Carolina 27650.

Received 22 June 1981.
0003-6935/82/010049-06$01.00/0.

transmitted to the gas within the photoacoustic cell produces the acoustic signal. If the sample is thin enough, thermal wave interference will affect the amplitude of this transmitted thermal wave and hence will affect the photoacoustic response.

The thermal waves within the filter backing, sample, and gas regions of the photoacoustic cell are illustrated in Fig. 1. In each region $\sigma_i = (1 + j)a_i$, where $j = \sqrt{-1}$ and a_i is the wave number of the thermal wave in the region i. As well as being dependent on the thermal properties of the material in which the thermal wave is propagating, a_i is dependent on the angular frequency ω at which the incident light beam is modulated; in particular, $a_i \propto \sqrt{\omega}$ or, equivalently, $\lambda_i \propto 1/\sqrt{\omega}$, where λ_i is the wavelength of the thermal wave in the region i. Therefore, we may vary the wavelength of the thermal waves in each of the three regions by varying the rate at which the incident light beam is modulated. The thermal waves initiated within the sample travel to the sample–backing and sample–gas boundaries. By applying the boundary conditions of temperature and flux continuity we may compute the thermal wave reflection coefficient R_i and the thermal wave transmission coefficient T_i at each of these boundaries. These coefficients have the form[6]

$$R_b = \frac{1-b}{1+b}, T_b = \frac{2}{1+b}, R_g = \frac{1-g}{1+g}, T_g = \frac{2}{1+g},$$

where

$$b = \sqrt{\frac{\rho_b C_b k_b}{\rho_s C_s k_s}}, g = \sqrt{\frac{\rho_g C_g k_g}{\rho_s C_s k_s}},$$

and where ρ_i, C_i, k_i are, respectively, the density (g/cm^3), the specific heat (joules/g K), and the thermal conductivity (watts/cm K) of the medium i. It is important to note that thermal waves are rapidly damped; in one period the wave will be attenuated by a factor of $\exp(-2\pi)$. The backing and gas regions of the cell are assumed to be thicker than one thermal wavelength in that region so that there is only a transmitted right traveling wave in the gas and a transmitted left traveling wave in the backing (see Fig. 1). However, if the sample is less than a thermal wavelength in thickness, the thermal waves within the sample will multiply reflect between the two boundaries, and the resulting thermal wave interference will affect the amplitudes of the transmitted waves.

To see how this occurs we let the incident light beam have intensity $\frac{1}{2}I_0[1 + \exp(j\omega t)]$. Since the photoacoustic signal arises from periodic temperature fluctuations we shall neglect the nonperiodic portion of the incident flux so that at any point x within the sample (see Fig. 1) the light absorbed between x and $x + dx$ is, in steady state, $\frac{1}{2}I_0\beta \exp(-\beta x)dx$, where β is

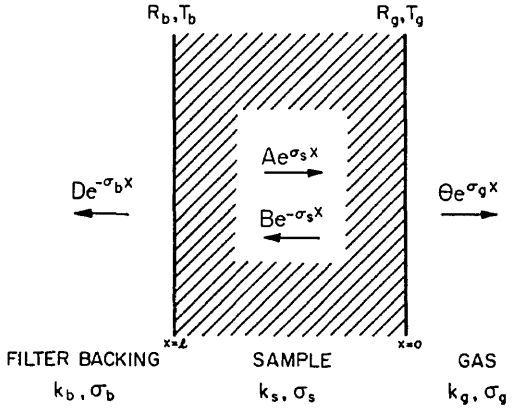

Fig. 1. Thermal waves in each of the three regions of the photoacoustic cell. Note that the direction of positive x is to the left. Light is incident from the right.

the absorption coefficient of the sample in cm^{-1}. (We assume that this absorbed radiation is converted nonradiatively into heat with a conversion efficiency of unity.) In our 1-D case, half of the energy will diffuse toward the gas and half will diffuse toward the backing. Hence the thermal waves initiated by light absorbed between x and $x + dx$ will have amplitude

$$\frac{\beta I_0 \exp(-\beta x)}{4k_s\sigma_s}dx.$$

These thermal waves travel through the sample, multiply reflecting between the sample-backing and sample-gas boundaries. Consider the thermal wave that originally travels toward the gas; it will contribute a series of transmitted terms at $x = 0$ equal to

$$\frac{\beta I_0 \exp(-\beta x)}{4k_s\sigma_s} T_g \{\exp(-\sigma_s x) + R_b R_g \exp[-\sigma_s(2l + x)] + \ldots + (R_b R_g)^n \exp[-\sigma_s(2nl + x)] + \ldots\}dx,$$

with $n = 0, 1, 2, \ldots$. Similarly, the thermal wave that originally travels toward the backing will contribute a series of transmitted terms at $x = 0$ equal to

$$\frac{\beta I_0 \exp(-\beta x)}{4k_s\sigma_s} T_g (R_b \exp[-\sigma_s(2l - x)] + (R_b R_g)R_b \times \exp[-\sigma_s(4l - x)] + \ldots + (R_b R_g)^n R_b \times \exp\{-\sigma_s[2(n + 1)l - x]\} + \ldots)dx.$$

Both of these series are geometric, with ratio $R_b R_g \exp(-2\sigma_s l)$. Summing both series and adding we obtain the amplitude of the thermal wave transmitted to the gas due to light absorbed between x and $x + dx$. Integrating from 0 to l we compute the amplitude θ of the thermal wave transmitted to the gas due to radiation absorbed from all points within the sample:

$$\theta = \frac{I_0\beta T_g}{4k_s\sigma_s}\left(\frac{\frac{1}{\beta+\sigma_s}\{1 - \exp[-(\beta+\sigma_s)l]\} + R_b \exp(-2\sigma_s l)\frac{1}{\beta-\sigma_s}\{1 - \exp[-(\beta-\sigma_s)l]\}}{1 - R_b R_g \exp(-2\sigma_s l)}\right).$$

A modest amount of algebra will convert this expression into the result obtained by Rosencwaig and Gersho.[5] The first term in braces represents the contribution from the direct thermal waves within the sample that originally travels toward the gas, and the second term represents the contribution from the thermal waves within the sample that initially travels toward the backing; hence the factor R_b. Whether there is a 180° phase shift for thermal waves reflecting from the sample backing boundary depends on the sign of R_b[6,7]; this will be an important consideration in interpreting our photoacoustic results.

A simple thermodynamical argument formulated by Rosencwaig and Gersho[5] may be used to establish the pressure variation within the photoacoustic cell due to this transmitted thermal wave. The photoacoustic signal will also depend on cell resonances, microphone response, etc.; this would make it exceedingly difficult to vary the modulation frequency and extract information regarding the sample in a systematic way. However, these effects may be removed from the data by choosing an appropriate reference sample. Since the signal associated with a thermally thick sample exhibits no structure due to thermal wave interference, the quantity

$$|R(\omega)| = \frac{S}{S_r},$$

where S and S_r are, respectively, the sample signal and reference signal at chopping frequency ω depends only on the thermal and absorptive properties of the material to be studied.

For simplicity we assume that the reference sample is thermally thick and opaque. In this case $R(\omega)$ becomes

$$R(\omega) = \frac{1 - \exp[-(\beta - \sigma_s)l] + R_b\left(\frac{\beta + \sigma_s}{\beta - \sigma_s}\right)\exp(-2\sigma_s l)\{1 - \exp[-(\beta - \sigma_s)l]\}}{1 - R_b R_g \exp(-2\sigma_s l)}.$$

If the wavelength of light used is such that $\beta \gg a_s$ over the range of modulation frequencies of interest so that $\exp(-\beta l) \sim 0$, $R(\omega)$ becomes

$$R(\omega) \simeq \frac{1 + R_b \exp(-2\sigma_s l)}{1 - R_b R_g \exp(-2\sigma_s l)}.$$

In this case the modulus of $R(\omega)$ is

$$|R(\omega)| = \sqrt{\frac{\left[\frac{1 + R_b \exp(-2a_s l)}{1 - R_b R_g \exp(-2a_s l)}\right]^2 - \frac{F}{R_g}\sin^2 a_s l}{1 + F \sin^2 a_s l}}, \quad (1)$$

where

$$F = \frac{4R_b R_g \exp(-2a_s l)}{[1 - R_b R_g \exp(-2a_s l)]^2},$$

and the phase difference between the reference and the sample signals is given by

$$\Delta\phi = \tan^{-1}\left\{\frac{-R_b(1 + R_g)\exp(-2a_s l)\sin 2a_s l}{1 - R_g[R_b \exp(-2a_s l)]^2 + R_b(1 - R_g)\cos 2a_s l}\right\}. \quad (2)$$

The reader should be aware that the thermal thickness $a_s l$ is proportional to the square root of the chopping frequency.

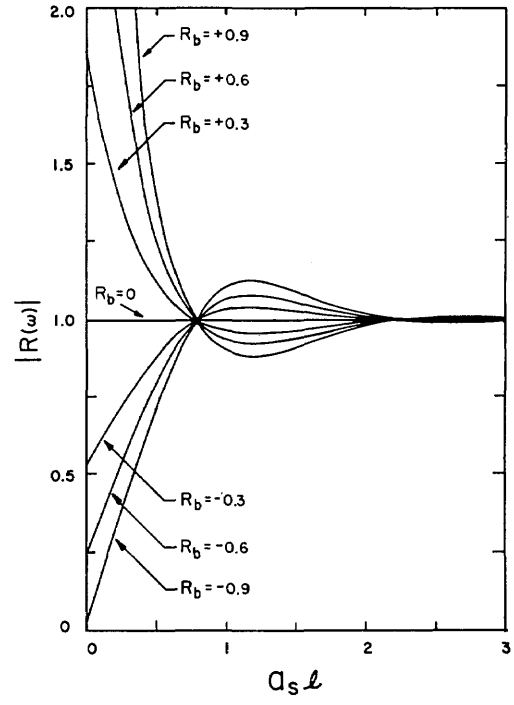

Fig. 2. Theoretical plot of the ratio $|R(\omega)| = S/S_r$ vs thermal thickness $a_s l$ for different values of the thermal wave reflection coefficient R_b at the sample–backing boundary, where S is the photoacoustic signal at angular modulation frequency ω due to a nonthermally thick sample, and S_r is the photoacoustic signal at ω due to a thermally thick sample of the same material. Both samples are opaque, and R_g has been taken to be 0.99. Note that $a_s l \propto \sqrt{\omega}$.

Figure 2 shows a plot of $|R(\omega)|$ vs thermal thickness $a_s l$ for a variety of values of R_b. The value of R_g was arbitrarily taken to be 0.99. If $R_b > 0$, thermal waves reflecting from the sample–backing boundary arrive at the sample–gas boundary in phase with the direct waves when the sample is thermally thin, resulting in constructive interference and a corresponding $|R(\omega)|$ that is greater than unity. As the thermal thickness increases, the thermal waves at the sample–gas boundary exhibit destructive interference with $|R(\omega)| < 1.0$, and eventually $|R(\omega)|$ approaches unity as the sample becomes thermally thick. Conversely, $R_b < 0$ results in destructive interference at the sample–gas boundary for the lower modulation frequencies; then constructive interference occurs with $|R(\omega)|$ approaching unity from above as the sample becomes thermally thick.

In Fig. 3 the phase difference between the reference and the sample signals is plotted vs thermal thickness for the same values of R_g and R_b used for Fig. 2. It is clear from Eq. (2) that the phase data contain thermal information; in particular, note that for $a_s l < 1.6$ the

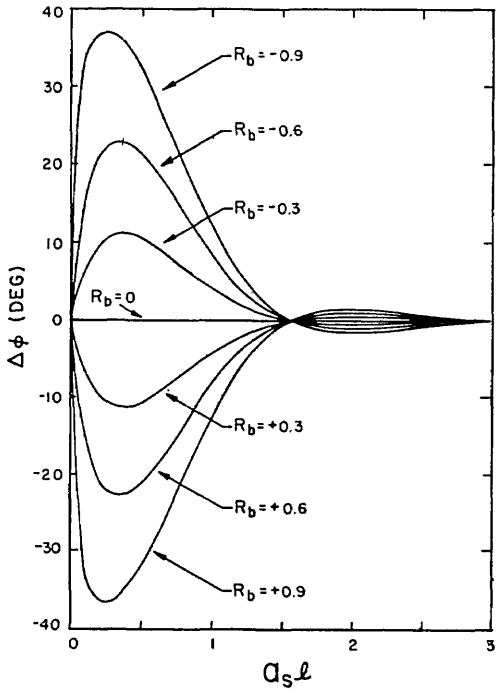

Fig. 3. Theoretical plot of the phase difference $\Delta\phi$ between the sample signal S and the reference signal S_r vs thermal thickness $a_s l$ for the same values of R_b and R_g for Fig. 2.

phase of the reference signal lags the phase of the sample signal when $R_b > 0$, and the phase of the reference signal leads that of the sample when $R_b < 0$.

The assumption that the sample is opaque is not a necessary assumption; this technique is applicable to a wide range of sample thicknesses and thermal properties, with the only limitation being the range of modulation frequencies compatible with the detection system. However, it should be mentioned that if a nonopaque sample is deposited on a reflecting substrate, the additional response due to light reflected from the substrate must be considered. It should also be mentioned that the simple theory outlined above does not account for oxide layers etc; if the existence of such layers perturbs the data, the theory must be modified accordingly.

It is not necessary to trace the entire curve for $|R(\omega)|$ or $\Delta\phi$ to obtain thermal or thickness information. Samples exhibiting very high thermal conductivity, such as silicon, could be analyzed by taking data only in the thermally thin regime. The quantity F in Eq. (1), which is denoted the coefficient of thermal wave finesse by analogy with the similar optical problem,[8] can become very large at low modulation frequencies if the product $R_b R_g$ is close to unity; this results from the fact that a thermal wave that is very long will multiply reflect many times between the sample–backing and sample–gas boundaries of a thermally thin sample before damping to zero. It should be easy to find substrates for which $R_b \rightarrow 1.0$ if the sample exhibits high thermal conductivity. (If the sample is physically thick enough to be self-supporting, a gas could be used for the substrate.) Samples of different thicknesses deposited on identical substrates would produce a family of curves emanating from a single y intercept

$$\left(\frac{1+R_b}{1-R_b R_g}\right)$$

resulting in a method for measuring the thickness of thin samples. The samples need not be optically flat, especially if the thermal wavelengths are very long over the range of modulation frequencies used for analysis. Finally, the use of both $|R(\omega)|$ and $\Delta\phi$ in conjunction with an iterative process may provide the most effective means of extracting thermal parameters from the data.

III. Experimental Methods

The detectors used in these measurements consisted of a small cylindrical cell 1.3 cm in diameter and 0.3 cm long equipped with a Knowles model BT 1759 microphone. The entrance window was glass, and the output window was opal glass. An RCA 1P39 photodiode placed immediately behind the opal glass was used to measure the fraction of light transmitted by each filter. Light from a He–Ne laser (Spectra-Physics model 125A) operating at 632.8 nm was modulated with a PAR model 192 variable speed chopper prior to impinging on the carbon particles contained on filter substrates mounted in the photoacoustic cell. The output of the microphone was measured by a PAR model 128A lock-in

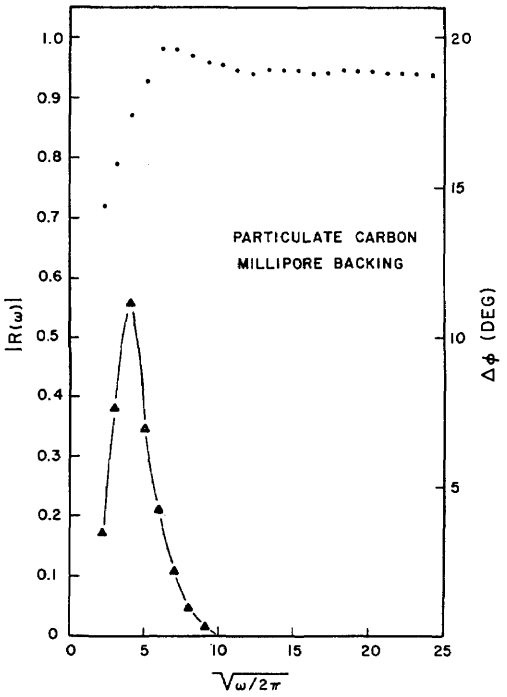

Fig. 4. Experimental plots of $|R(\omega)|$ (dots) and $\Delta\phi$ (triangles) vs the square root of the modulation frequency for samples of particulate carbon deposited on Millipore substrates.

amplifier, and the output of the photodiode was measured with a PAR model HR8 lock-in amplifier. The carbon particles were generated by burning propane and oxygen in a chamber flushed with a nine-to-one mixture of nitrogen and oxygen. A dichotomous sampler (Environmental Research Co.) was used to deposit the carbon particles on filter substrates at a flow rate of 16.7 liters/min. The Teflon filters were stored in a dessicator for at least 48 h prior to weighing on a Metler balance capable of yielding filter weights before and after loading to within ± 25 μg.

IV. Experimental Results

In Fig. 4 we show a plot of $|R(\omega)|$ vs $(\omega/2\pi)^{1/2}$ (circles) along with a plot of $\Delta\phi$ vs $(\omega/2\pi)^{1/2}$ (triangles) for a particulate carbon sample deposited on a Millipore substrate. Note that there is apparently no ambiguity in talking about thermal waves in particulate samples such as these; the thermal wavelength is much greater than the particle size or particle separation for all modulation frequencies under consideration. However, a practical difficulty was encountered in preparing a reference sample thick enough to be thermally thick at the lower modulation frequencies. The amount of carbon deposited on this filter was probably in the range of tens of milligrams of carbon per square centimeter (gravimetric analysis of Millipore filters was not possible since these filters were bonded onto frames), and it appears that it is not possible to prepare a deposit of this magnitude that has the same thermal properties as a more lightly loaded sample (typically tens of micrograms per square centimeter). This resulted in a asymptotic value that differed from unity; therefore, the sample deposit was made sufficiently large to have thermal properties that approached that of the reference (asymptotic value ~0.94) and yet sufficiently small to show the necessary structure in the range of modulation frequencies ($f > 5$ Hz) compatible with our detection system. Consequently, a detailed comparison of theory and experiment is not attempted at this time. However, the overall structure of the experimental data shown in Fig. 4 compares favorably with the theoretical results shown in Figs. 2 and 3 for $R_b < 0$ (actually, there is reasonable agreement with the plot for reflectivity $R_b = -0.3$). It should be mentioned that problems such as these would probably be absent for nonparticulate samples.

The role of the backing material is illustrated in Fig. 5, where the photoacoustic signals from different carbon samples deposited on three commonly used substrates are plotted against the optical thickness of each deposit (determined from transmission measurements). All loadings in these plots are in the 0–120-μg/cm range; thus the effects due to large loadings discussed above are absent in these data. For all three substrates the photoacoustic signal at 100 Hz continues to rise even after the samples become optically opaque ($\beta l > 3$), indicating again that $R_b < 0$. The thermal waves at the sample–gas boundary interfere destructively for the thinner samples and interfere more and more constructively as the sample thickness increases, causing the photoacoustic signal to continue to rise instead of saturating. Increasing the modulation frequency to 1600 Hz increases the thermal thickness of all the samples; the difference in the two sets of data is evident. Note that the lack of saturation in the 100-Hz photoacoustic data is much more severe for samples collected on Millipore and Nuclepore filters than for those collected on Teflon filters; this indicates that R_b is much closer to -1.0 for carbon samples deposited on Millipore and Nuclepore substrates than for carbon samples deposited on Teflon substrates. This is also evident from the fact that the magnitude of the photoacoustic signal is larger for a carbon sample deposited on Teflon than for the same sample deposited on Millipore or Nuclepore. (All 100 Hz data are interconsistent in magnitude.)

As a final verification that thermal wave interference is responsible for the structure shown in Fig. 4, we show in Fig. 6 a plot of photoacoustic signal vs optical thickness for a modulation frequency of 3000 Hz for carbon samples deposited on Teflon filters. In both cases the thermal thickness is varied; in Fig. 4 the thermal thickness of a single sample is varied by changing the modulation frequency, and in Fig. 6 the thermal thickness is varied by actually changing the physical thickness. The similarities between Figs. 4 and 6 are evident, and the influence of thermal wave interference on the photoacoustic signal is clearly demonstrated.

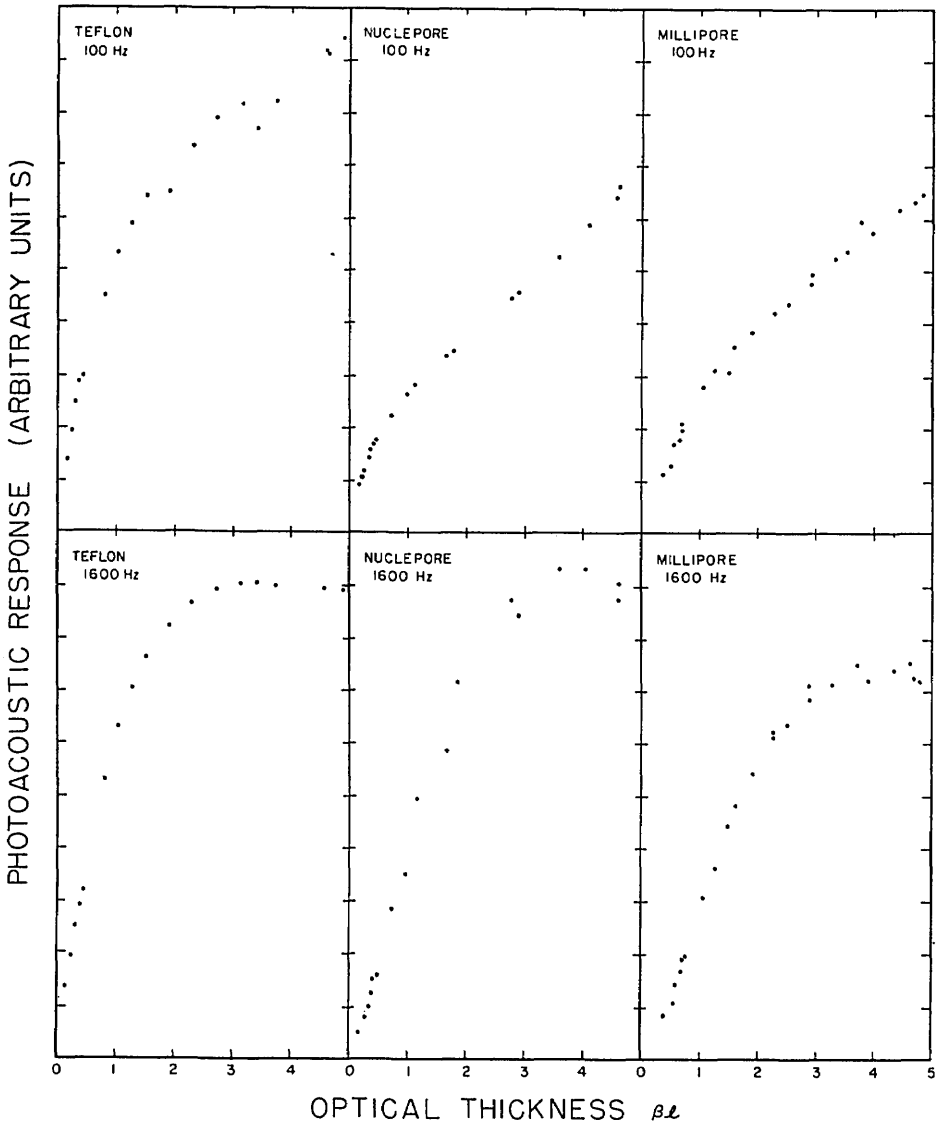

Fig. 5. Photoacoustic signal vs optical thickness βl (proportional to sample thickness) for modulation frequencies of 100 and 1600 Hz due to samples of particulate carbon deposited on three different substrates: Teflon, Nuclepore, and Millipore.

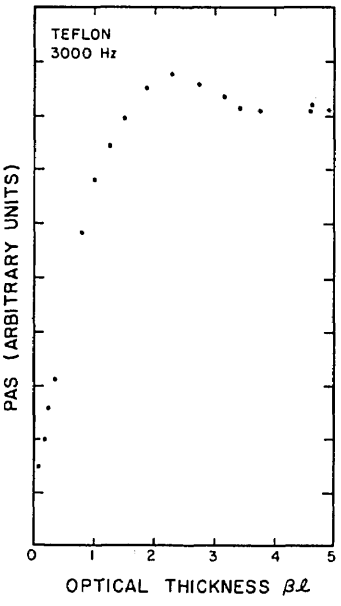

Fig. 6. Photoacoustic signal vs optical thickness βl due to carbon particles deposited on Teflon substrates analyzed at a modulation frequency of 3000 Hz. In Fig. 4 the structure in the photoacoustic signal due to thermal wave interference is illustrated by varying the wavelength of the thermal waves generated within the sample; in Fig. 6 this structure is illustrated by varying the physical thickness (and hence the thermal thickness) of different carbon deposits analyzed at a single modulation frequency.

V. Conclusions

A procedure for extracting information on the thermal properties of a sample has been suggested, and experimental data have been presented that compare favorably with the theoretical predictions. This technique is potentially a powerful and straightforward application of the photoacoustic effect in condensed phase.

This work was supported in part by the Environmental Protection Agency under grant R805332 02.

References

1. C. A. Bennett, Jr., and R. R. Patty, Appl. Opt. **20**, A60 (1981).
2. C. A. Bennett, Jr., and R. R. Patty, (in press, J. Photoacoustics).
3. H. S. Carslaw and J. C. Jaeger, *Conduction of Heat in Solids* (Oxford U.P., Oxford, 1959), p. 64.
4. P. M. Morse and K. U. Ingard, *Theoretical Acoustics* (McGraw-Hill, New York, 1968), p. 479.
5. A. Rosencwaig and A. Gersho, J. Appl. Phys. **47**, 64 (1976).
6. F. A. McDonald, Am. J. Phys. **48**, 41 (1980).
7. F. A. McDonald and G. C. Wetsel, Jr., J. Appl. Phys. **49**, 2313 (1976).
8. M. Born and E. Wolf, *Principles of Optics* (Macmillan, New York, 1964), p. 323.